A plain linear rule for fatigue analysis under natural loading considering the coupled fatigue and corrosion effect

I. Calderon-Urízar-Aldaca, E. Briz, M.V. Biezma, I. Puente

PII: S0142-1123(19)30017-9
DOI: https://doi.org/10.1016/j.ijfatigue.2019.01.008
Reference: JIJF 4951

To appear in: *International Journal of Fatigue*

Received Date: 23 October 2018
Revised Date: 12 January 2019
Accepted Date: 20 January 2019

Please cite this article as: Calderon-Urízar-Aldaca, I., Briz, E., Biezma, M.V., Puente, I., A plain linear rule for fatigue analysis under natural loading considering the coupled fatigue and corrosion effect, *International Journal of Fatigue* (2019), doi: https://doi.org/10.1016/j.ijfatigue.2019.01.008

A plain linear rule for fatigue analysis under natural loading considering the coupled fatigue and corrosion effect

I.Calderon-Urízsar-Aldaca[1*], E. Briz[2], M. V. Biezma[3], I.Puente[4]

[1] Tecnalia Research and Innovation, Sustainable Construction Division, Technological Park of San Sebastián, Paseo Mikeletegi nº2, Ed. M2, San Sebastian, Spain.

[2]Dept. of Mechanical Engineering, Faculty of Engineering, University of the Basque Country (UPV/EHU), Plaza Ingeniero Torres Quevedo 1, 48013 Bilbao, Spain. ORCID 0000-0003-3933-3585.

[3]Dept. of Earth and Materials Science and Engineering, University of Cantabria, UC. C/ Dique de Gamazo 1, 39004 Santander, Spain. ORCID:0000-0002-0709-7656.

[4]Dept. of Mechanical Engineering, Institute of Civil Engineering, Tecnun (University of Navarra), Paseo Manuel de Lardizabal 13, San Sebastián, 20018, Spain

*Corresponding author: E-mail address: inigo.calderon@tecnalia.com (I. Calderon-Uriszar-Aldaca).

Abstract

Fatigue under variable amplitude loading is currently assessed by applying the Palmgren-Miner linear rule in structural standards. However, this linear rule is inadequate in natural scenarios with coupled fatigue and corrosion effects, because the coupled corrosion-fatigue process synergistically accelerates deterioration. In view of the absence of specifications for the coupled fatigue-corrosion effect in structural standards, the objective here is to develop a simple and practical correction factor that will ensure a conservative linear summation of damage, taking the corrosion-fatigue effect into account. The theoretical consistency and the feasibility of the new adapted rule are tested in a case study.

Keywords

Corrosion fatigue; corrosion pushing factor; reinforced concrete structures;

Highlights

- Review of linear and non-linear rule approaches to coupled corrosion-fatigue damage.
- Non-linear approach suitable for coupled corrosion-fatigue processes.
- Linear-rule determination of acceleration factor for equivalent damage.
- Linear-rule for coupled corrosion-fatigue effect considering structural reliability.
- Demo-case upholds simplicity and suitability of a representative structural element.

1. Introduction

A state-of-the-art examination of the fatigue life of welded structures in corrosive marine environments that seeks to identify corrosion fatigue in structural details is

described in certain offshore standards, such as DNV-OS-J101 [1], DNV-RP-C203 [2] and BS EN ISO 19902 [3]. However, since the aforementioned standards have been applied to the design of offshore platforms and wind-turbine generators, some engineers may wish to extend the scope of these techniques to inland structures. See [4].

Nevertheless, fatigue in the structural details of civil works, buildings, and industrial facilities is described in the standards of both the Eurocodes, in Europe [5], and the AISC, in the USA [6], which have become global references. Thus, even considering that offshore platforms and aerogenerators had equivalent structural details [], especially with regard to geometries, without considering steel grades and welding procedures, as per the corresponding standards, such an approach would present several drawbacks. Namely:

a) Inland structures up to 5 km from the coast are exposed to corrosive atmospheric conditions, even though they are less corrosive than offshore marine environments. In addition, there are several other electrolyte sources, such as de-icing salts, traffic emissions, chemicals in and nearby industrial facilities, chlorides in swimming pools and water processing plants, and biological corrosion, among others (exposure classes that are well defined in the standards). The notion that the provisions for off-shore platforms could be applied to inland structure is neither suitable nor reasonable; in many cases, it would be too conservative and onerous on the budget, while in others it would simply be unsafe. Feasibility case studies developed in this paper on corrosion following the exposure of rebars to marine environments provide useful information for demonstration purposes. However, in consideration of the range of steel grades in inland structures and the environmental conditions to which they are exposed, an engineer will need to assess corrosion rates with more flexible parameters.

b) Specific frequencies will also vary: for example, the Davenport spectra (and derivatives) can be valid for wind throughout the service life of a structure, with a mean frequency equal to the square root of the 4^{th}-order moment divided by the 2^{nd}-moment of the Power Spectral Density function in the frequency domain, when considering stationary and ergodic fatigue loading process (as with waves). In cases where structures are subjected to different sources of loading, the stationarity and ergodicity of the process is compromised and cannot be considered in Gaussian terms. Corrosion is time dependent and fatigue is cycle dependent, so process frequency is therefore crucial. The corrosion process in structures subjected to lower frequencies (i.e. loading peaks produced by a passing train) is dominant over fatigue in corrosion-fatigue, while in others with higher frequencies (i.e. aerogenerators), fatigue is dominant, as the corrosion depends on long-term chemical reactions. Thus, all things considered, engineers will need to apply very flexible parameters for frequency in their designs.

c) Moreover, loading sources will differ from one structure to another, resulting in different stress cycles. The main design guideline for a high-rise building could be seismic-related, while traffic loads would be essential for the design of road bridges, and gantry crane loads in the design of industrial facilities. Hence, non-Gaussian histograms with very few cycles would be used at higher ranges and the vast majority of cycles at lower ranges, where corrosion is the most damaging

mechanism. In other words, an engineer will find heavier structural details in several inland structures that have been overdesigned for dominant loading (500 return period seisms and 50 return period storms), which have to endure very low stress range cycles from other loadings and, much more occasionally, intensive cycles. Nevertheless, within the same structure, other structural details that are not designed to resist such dominant loads could suffer higher stress ranges from the same loading values. Therefore, an engineer will need flexibility to consider several stress ranges for different structural details.

d) Finally, the service life of different structures is also a point to consider in deterioration processes. While a bridge or hospital design life is up to 100 years, the building's life might be 50 years and an aerogenerator could be half as long.

Hence, current structural standards for inland structures [5, 6] incorporate the assumption of sufficient corrosion protection, although in other cases the provisions fall outside of the desired scope. According to the recommendations of the aforementioned standards, the fatigue damage of each structural detail is derived by means of S-N curves [7] and accumulated by the Palmgren-Miner [8, 9] linear rule. This method is not the most accurate, but is feasible and practical for structural engineers with no specialization in fatigue, and sufficiently conservative to be safe. However, at the end of the day, in the presence of a corrosive environment, there are no alternative rules, and some engineers may tend to design for inert environments and simply gloss over the problem.

Thus, an accelerating coefficient determination method is presented in this manuscript, to take into account corrosion within the same paradigm of the S-N curve [[7] plus the Palmgren-Miner [8, 9] linear rule. Its added value is that it enables safer fatigue forecasts, by considering the corrosiveness of the environment, while keeping knowledge transfer to the sector and ease of adoption both feasible and practical. A coefficient taking into account:

- Corrosion kinematics, by means of a corrosion rate;
- Mean frequency of the process;
- Structural detail geometry, by means of geometry factor;
- Stress ranges;
- Steel grades, by means of Paris Law constants, the Griffith's threshold, and critical values; and,
- Service life.

Besides, this method described in this manuscript presents an open rather than a closed solution, which can be enriched by further findings in terms of corrosion kinematics, corrosive scenarios, steel grades, and loading combinations, among others. It is a method with which an accelerating coefficient may be derived from the available physical knowledge. Rather than a false conclusion based on further research yet to be completed, it responds to the need for a practical and feasible method for the progressive incorporation of research findings.

Fatigue damage, as mentioned above, is widely assessed with the Palmgren-Miner [8, 9] rule. However, fatigue depends on many factors such as the stress range,

the sequential order of cycles and the corrosive environment, which are not factored into a linear approximation. Consideration of these effects would require a non-linear rule, which is quite complex and therefore less practical. In a previous work [10], a disorder-pushing factor was defined, to consider the sequential order effect in the Palmgren-Miner rule. Continuing along those same lines, a corrosion-pushing factor for the estimation of corrosion-fatigue is now presented in this paper. Hence, since the effect of corrosion on fatigue strength of metallic materials depends also on load level as well as type of loading, i.e. constant versus variable amplitude loading, the influence of this variable needs to be analyzed in depth in future works.

Corrosion fatigue models [11, 12, 13, 14] have been developed in recent research. Nevertheless, the difficulty of the solutions to such equations has halted any further practical development in the community. Among the first of such models, FATOXFLU [15] divides the fatigue process into two stages: micro-initiation and micro-propagation, considering only corrosion in the first one.

When corrosion fatigue occurs over some cycles, the crack size will increase due to two sources: mechanical propagation and corrosion pitting. The first relates with the cycles of loading and the second with the time that elapses during those cycles, while under constant electrolyte presence. Therefore, mechanical propagation and corrosion pitting are related by means of load frequency. It is evident that the only possible effect in a process with a frequency of 0 is corrosion, while the corrosion effect would be negligible in processes with very high frequencies. Hence, as the loading frequency decreases, there is a lengthier time between cycles for corrosion reactions and ion transfer, which increases the crack propagation rate [13, 16, 17, 18, 19]*;* and the opposite also holds true.

Thus, considering both the Paris Law [20] and the Griffith's threshold [21], the crack propagation rate for a plain metallic sheet loaded at a given tensile stress with a central initial crack (2·a) can be estimated from eq. (1). Then, after integrating this equation, the final crack size can be obtained from eq. (2)

$$\frac{da}{dN} = A \cdot (\Delta\sigma \cdot \sqrt{\pi a})^m \tag{1}$$

$$\left[\frac{2}{2-m} \cdot a^{\frac{2-m}{2}}\right]_{a_0}^{a_f} = A \cdot \Delta\sigma^m \cdot \pi^{m/2} \cdot [N]_{N_0}^{N_f} \tag{2}$$

Where (a) is the crack size, (A) and (m) are the material constants, (N) is the number of cycles, (Δσ) is the stress range, (N_0) and (N_f) are the initial and final amount of cycles, and (a_0) and (a_f) are the initial and final crack sizes.

If the corrosion process stops at a certain crack size, the crack will propagate due to mechanical growth defined in eq. (2). Moreover, if the mechanical process ceases, the corrosion process will follow its own kinematics, such as the one presented in eq. (4). Hence, if the coupled fatigue-corrosion process is interrupted, the metal will be repassivated and a new mechanical fatigue process will start, at which point the final crack size of the process that had been interrupted would be the initial crack size of the process that was recommencing, following eq. (2).

Now, it may be said that the corrosion effect pushed the process of mechanical fatigue, increasing the number of effective cycles, as plotted in Figure 1. The crack

propagates from A to B, as described in eq. (3), as the mechanical cycles, (ΔN_m), increase, over a total time lapse, (Δt), at a known frequency, (f). During this time, the corrosion contributes to crack propagation at a certain corrosion rate (v_c), from B to B', as defined by eq. (4) and depicted in Fig.1. At this point, the total crack size (Δa_t) can be calculated with eq. (5). Thus, starting with the same crack size, if the fatigue process were strictly mechanical, the total crack size growth (Δa_t) would be achieved at (ΔN_t), at point C. Hence, the final crack size, as in eq. (6), can be found in combination with eq. (2), (ΔN_t) at point C; see eq. (7). Then, the cyclic loading period will start at C, with a higher crack size growth rate, which precisely reflects the synergic effect of corrosion fatigue.

$$a_f = \left[\frac{2-m}{2}\cdot a\cdot \Delta\sigma^m \cdot \pi^{m/2}\cdot \Delta N_m + a_0^{\frac{2-m}{2}}\right]^{2/2-m} \tag{3}$$

$$\Delta a_c = v_c \cdot \Delta t = v_c \cdot \frac{\Delta N_m}{f} \tag{4}$$

$$\Delta a_t = \Delta a_m + \Delta a_c \tag{5}$$

$$a_f = a_0 + \Delta a_t \tag{6}$$

$$\Delta N_t = \frac{\left(\frac{2}{2-m}\right)\cdot\left\{\left[\left(\frac{2-m}{2}\cdot A\cdot\Delta\sigma^m\cdot\pi^{m/2}\cdot\Delta N_m + a_0^{\frac{2-m}{2}}\right)^{\frac{2}{2-m}} + \frac{v_c}{f}\cdot\Delta N_m\right]^{\frac{2-m}{2}} - a_0^{\frac{2-m}{2}}\right\}}{A\cdot\Delta\sigma^m\cdot\pi^{m/2}} \tag{7}$$

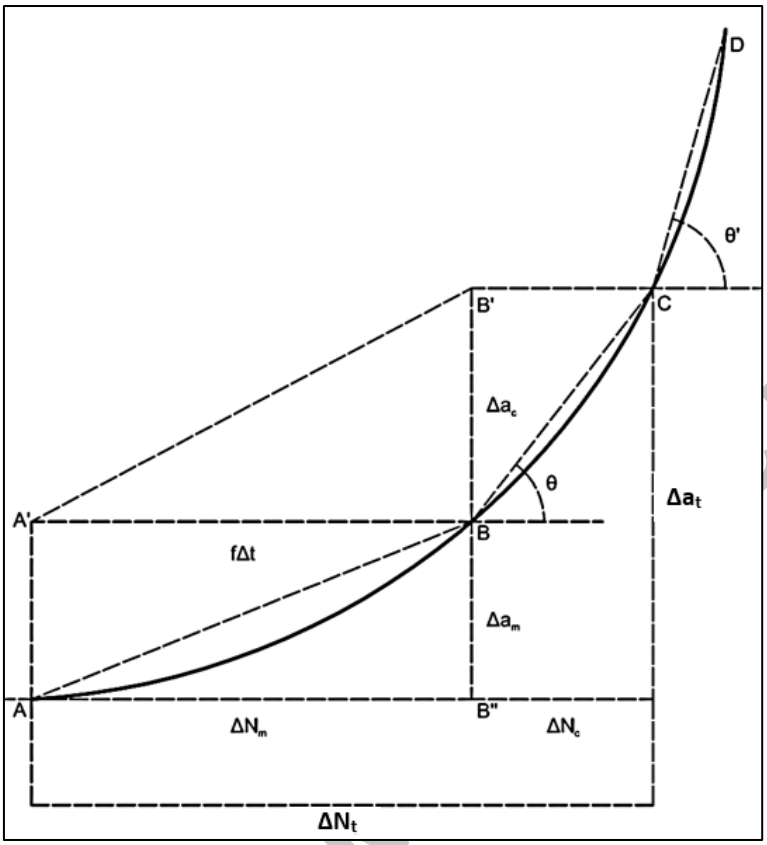

Figure 1 Cyclic pushing effect, due to synergic corrosion fatigue.

The following observations may be verified in Eq. (7):

- With no corrosion v_c=0, it would therefore follow that ΔN_t=ΔN_m.
- As f increases ΔN_t decreases, which as previously mentioned is consistent with physical observations and closer to ΔN_m.
- A Corrosion Pushing factor is defined in eq. (8). This factor will be closer to the real fatigue-corrosion situation with shorter intervals between cycles.

$$F_{CP} = \frac{\Delta N_t}{\Delta N_m} \tag{8}$$

- F_{CP} is higher in the initial stages of the corrosion fatigue process, in accordance with the predictions of the FATOXFLU model [15]. FATOXFLU defines a micro-initiation stage, in which the mechanical process is less intense, hence, the corrosion pushing factor is stronger.
- Regarding the variation of corrosion rate, or even the repassivation of the element, from the point of view of the structural safety, there are two approaches. The first one, more conservative, is to consider an upper bound of corrosion rate and do the calculations with that one taken as constant for the whole process. The second one, more accurate, to discretize the process in blocks of cycles and consider the corrosion rate constant block by block. Nevertheless, as already said, the corrosion contribution is critical in early stages of the process and almost negligible near the end.

2. Theoretical generalization

All the previous equations have been developed for the simplest general case with an initially defined crack size (2·a). However, the initial crack size in real situations is not defined and the equations must therefore be adapted by the addition of a geometrical factor. Besides, that simple case was based in tension stress process, namely fracture mode I, but the methodology could be analogously applied to the other modes II and III related with shear and torsion stresses, even more sensitive to corrosion in some cases where the S-N curves present lower slopes.

A particular case of reinforced concrete steel rebars is considered, to show the development of a corrosion pushing factor. In such cases, the initial crack is due to a cold-forming, rib-threading process or a previous stress corrosion cracking phenomenon. In this paper, a suitable fatigue-corrosion pushing factor is proposed for reinforced concrete rebars, with the aim of easily providing a quantifiable fatigue-corrosion damage index for structural engineering calculations.

Just as a clarification, the rebar was a case for demonstrative purposes only, but the methodology remains applicable to other structural details. It was selected for being a simple structural detail among the ones presented with S-N curves given in Eurocode 2 and first ECCS seminal fatigue guide [22, 23]. Thus, since it is based on the standardized procedure for rebar fatigue, it remains valid within the same scope.

However, while it is true that a rebar is not an isolated element within a reinforced concrete structure, as a composite material, it is also true that at the end of the day a rebar could suffer tension stress cycles and that the concrete around it tends to crack under tension, mainly perpendicularly to it and where suffering more tension, allowing the corrosive electrolyte to enter through the cracks and start pitting corrosion at localized spots where the cracks exceed the coverage, such spots concentrates stresses and the fatigue-corrosion starts. Therefore, the boundary conditions for this case keeps realistic enough.

Aggressive environment represents one of the biggest problems for the durability of reinforced concrete (RC) structures. Apart from being exposed to a corrosive environment, they must withstand their static and, where applicable, dynamic design loads. Some RC structures, such as bridges and offshore structures are simultaneously subjected to fatigue loading and corrosive environments, which causes unexpected corrosion fatigue failure. Many studies have been performed to understand the behaviour of corrosion fatigue. However, most of them study the damage caused to previously corroded specimens [25, 26]; ignoring the simultaneous effects of the corrosion process and cyclic loading which together cause greater damage than they do separately.

The process followed in the introduction section functions for a flat sheet with a centred and well-defined initial crack. However, in RC structures, the metallic specimen is a steel rod with a radius (r) and the initial crack is usually unknown, which renders the above process useless. By adding a geometric factor, eq. (9), to the Griffith threshold [21, 27], eq. (7) can be adapted to RC bars, as shown in eq. (10).

$$Y(a) = \frac{1.84}{\pi} \cdot \frac{\left[\tan\left(\frac{\pi \cdot a}{4 \cdot r}\right)/\left(\frac{\pi \cdot a}{4 \cdot r}\right)\right]^{0.5}}{\cos\left(\frac{\pi \cdot a}{4 \cdot r}\right)} \cdot \left\{0.752 + 2.02 \cdot \left(\frac{a}{2 \cdot r}\right) + 0.37 \cdot \left[1 - \sin\left(\frac{\pi \cdot a}{4 \cdot r}\right)\right]^3\right\} \quad (9)$$

$$\Delta N_t = \frac{\left(\frac{2}{2-m}\right) \cdot \left\{\left[\left(\frac{2-m}{2} \cdot A \cdot \Delta\sigma^m \cdot Y_{mean}^m \pi^{m/2} \cdot \Delta N_m + a_0^{\frac{2-m}{2}}\right)^{\frac{2}{2-m}} + \frac{v_c}{f} \cdot \Delta N_m\right]^{\frac{2-m}{2}} - a_0^{\frac{2-m}{2}}\right\}}{A \cdot \Delta\sigma^m \cdot Y_{mean}^m \cdot \pi^{m/2}} \quad (10)$$

The value of the two constants, (A) and (m), depend on material and structural detail. This case study considers a plain carbon steel rebar, the values of which are: $A=2 \cdot 10^{-13}$ y m=3, [28]. Thus, eq. (11) is derived by substituting the above values in eq. (10). The geometric factor value is a mean value for each interval, noted as (Y_{mean}).

$$\Delta N_t = \frac{\left[\left(-10^{-13} \cdot \Delta\sigma^3 \cdot Y_{mean}^3 \pi^{3/2} \cdot \Delta N_m + a_0^{\frac{-1}{2}}\right)^{-2} + \frac{v_c}{f} \cdot \Delta N_m\right]^{\frac{-1}{2}} - a_0^{\frac{-1}{2}}}{10^{-13} \cdot \Delta\sigma^3 \cdot Y_{mean}^3 \cdot \pi^{3/2}} \quad (11)$$

Having obtained (ΔN_t), a value for the (F_{EC}) is given by eq. (8). Nevertheless, the lower the (ΔN_m) value, the more accurate the results, such that the most rigorous results are given by ΔN_m=1. (F_{EC}) also depends on (a_o), which means that in a study of more than one stage, the initial crack size for one stage is the final crack size of the previous stage. Therefore, for any moment, (F_{EC}) is defined as expressed in eq. (12). However, (F_{EC}) depends on the initial crack size, derived from fracture mechanics, a fact which complicates the exact estimation of (F_{EC}).

$$F_{EC}(a, v_c, f, \sigma, \phi) = \frac{\left[\left(-10^{-13} \cdot \Delta\sigma^3 \cdot Y_{mean}^3 \pi^{3/2} + a_0^{\frac{-1}{2}}\right)^{-2} + \frac{v_c}{f}\right]^{\frac{-1}{2}} - a_0^{\frac{-1}{2}}}{10^{-13} \cdot \Delta\sigma^3 \cdot Y_{mean}^3 \cdot \pi^{3/2}} \quad (12)$$

3. Plain Methodology

In structural engineering practice, S-N curves [7] are widely used to define the number of cycles until failure under fatigue loading cycles. The S-N curves of specimens exposed to a corrosive environment will therefore need to be defined first of all, followed by the corrosion-pushing factor, which may be calculated by dividing the S-N curve in an inert environment by the S-N curve for corrosion.

Just for note, it is worthy to mention that some manuscripts [29, 30] model the corrosion as a uniform element weight loss following an exponential law with time. Then, the reduced sections at several corrosion stages are analyzed by FEM under the same loads and the corrosion is thereby translated into stress increments to be compared with mechanical S-N curves of the same detail. Such approach is certainly a step forward to consider coupled corrosion, but it is not consistent with fracture mechanics and, therefore, neglects some important issues:

• A global thickness loss of a few μm could not seem a big deal in terms of global stress increment in a bridge deck. Nevertheless, when attending it locally at crack tip, it produces two effects: high stress concentration and cycle saving to reach the same crack size. Being the later more pronounced in initial stage, when each cycle barely contributes to crack growth.

• A corrosion pit produces stress concentration, overcoming the crack threshold and starting a fatigue crack. Simultaneously, a fatigue crack presents an anode at the tip and a cathode at the outer surface, meaning corrosion concentration at the tip and corrosion passivation at the surface.

• The S-N curves relate each stress range with the corresponding cycles until failure. However, in terms of crack propagation, having a look to Paris Law, the fatigue crack grows very slowly at the beginning, faster thereafter and suddenly at the end. This means that fatigue damage is not uniformly distributed along such cycles until failure, it is much higher at the end of the process and lower at the beginning instead, when the corrosion contribution is higher correspondingly. Thus, coupled corrosion can't be translated only into a stress increment of the same curve, computing the cycle profit in terms of the difference.

Hence, a methodology suitable to consider coupled corrosion fatigue by Palmgren-Miner linear rule must be consistent with fracture and fatigue theory.

3.1 Derivation of S-N Curves from the Paris Law

Every stress range (S) must be related to its corresponding number (N) of cycles until failure, in order to be able to define an S-N curve, which can be theoretically derived from the Paris law [20, 31, 23], previously defined in eq. (1). Hence, before the definition of such curves for each environment, some variables are required. EHE-08 and EN 1992-1-1:2013 [32, 22] both specify a maximum tensile stress of 300 MPa with a stress range of 150 MPa after 2,000,000 cycles in the case of B-500-SD rebars [33]. In contrast, the S-N curves in [22] are defined by a stress range of 162.5 MPa after 1,000,000 cycles. The number of 1,000,000 cycles was finally selected, following the comparison of the S-N curves obtained by applying the fracture mechanics method with the S-N curves obtained with the method in EN 1992-1-1 [22].

Thus, Table 1 summarizes the parameters for B-500-SD, where (A) and (m) are the constants in the Paris law for steel rebars taken from the literature [28], and (K_{IC}) coming from [34]. Besides, Table 2 summarizes the minimum and the maximum tensile ratio (R) depending on both the stress range ($\Delta\sigma$), and the corresponding threshold stress intensity factor (K_{th}) both of which are derived from equations (13) and (14), taken from [35, 36]. Just as a clarification, with enough cycle amount (giga-cycles), even under inert environment conditions, failure finally occurs and threshold or fatigue limit concepts loss their sense [37]. Nevertheless, when considering the much lesser expected number of cycles during service life of an infrastructure such as a building or a bridge (mega-cycles), with low natural frequencies, it is needed threshold stress intensity and corresponding crack size to have any expectancy of failure.

$$\Delta K_{th} = 191\ Nmm^{-3/2} \quad R \leq 0.17 \tag{13}$$

$$\Delta K_{th} = 222.4(1 - 0.85R)\ Nmm^{-3/2} \quad R > 0.17 \tag{14}$$

Table 1: Parameters defined for the calculation of cycles until failure of a B-500-SD rebar specimen.

σ_m [Mpa]	225
K_{IC} [Nmm$^{-3/2}$]	3000
[19]A	2.00E-13
m	3

Table 2: Tensile range, minimum/maximum tensile ratio and threshold stress intensity factors under analysis.

Δσ [Mpa]	R	ΔKth [Nmm$^{-3/2}$]
50	0.72727273	84.91636364
100	0.53846154	120.6092308
150	0.4	146.784
162.5	0.37096774	152.2722581
200	0.29411765	166.8
250	0.21052632	182.6021053
300	0.14285714	191
350	0.08695652	191
400	0.04	191
450	0	191
500	-0.03448276	191

3.2 Deriving threshold crack size, a_{th}, and critical crack size, a_{cr}.

A minimum crack size is needed for crack propagation (a_{th}), below which the stress concentration at the tip of the crack is insufficient for propagation to take place [38]. The minimum crack size is obtained from eq. (15), which has been defined based on the Griffith criterion [21], considering the geometric factor Y(a)=f(a) as defined in eq. (9), introduced in (15) as Y(a_{th})=β. The values obtained, for different diameters, are summarized in Table 3 and plotted in Figure 2 [39].

$$a_{th} = \frac{1}{\pi}\left(\frac{\Delta K_{th}}{\beta \Delta \sigma}\right)^2 \tag{15}$$

Table 3: Minimum threshold crack size values (a_{th}) [mm]

a_{th}						
Δσ	**Φ10**	**Φ12**	**Φ16**	**Φ20**	**Φ25**	**Φ32**
50	1.25	1.3	1.36	1.39	1.42	1.44

100	0.72	0.73	0.74	0.75	0.76	0.76
150	0.52	0.52	0.53	0.53	0.53	0.54
162.5	0.48	0.49	0.49	0.5	0.5	0.5
200	0.4	0.41	0.41	0.41	0.41	0.41
250	0.33	0.33	0.33	0.34	0.34	0.34
300	0.28	0.28	0.28	0.28	0.28	0.28
350	0.22	0.22	0.22	0.22	0.22	0.22
400	0.17	0.17	0.17	0.17	0.17	0.17
450	0.14	0.14	0.14	0.14	0.14	0.14
500	0.11	0.11	0.11	0.11	0.11	0.11

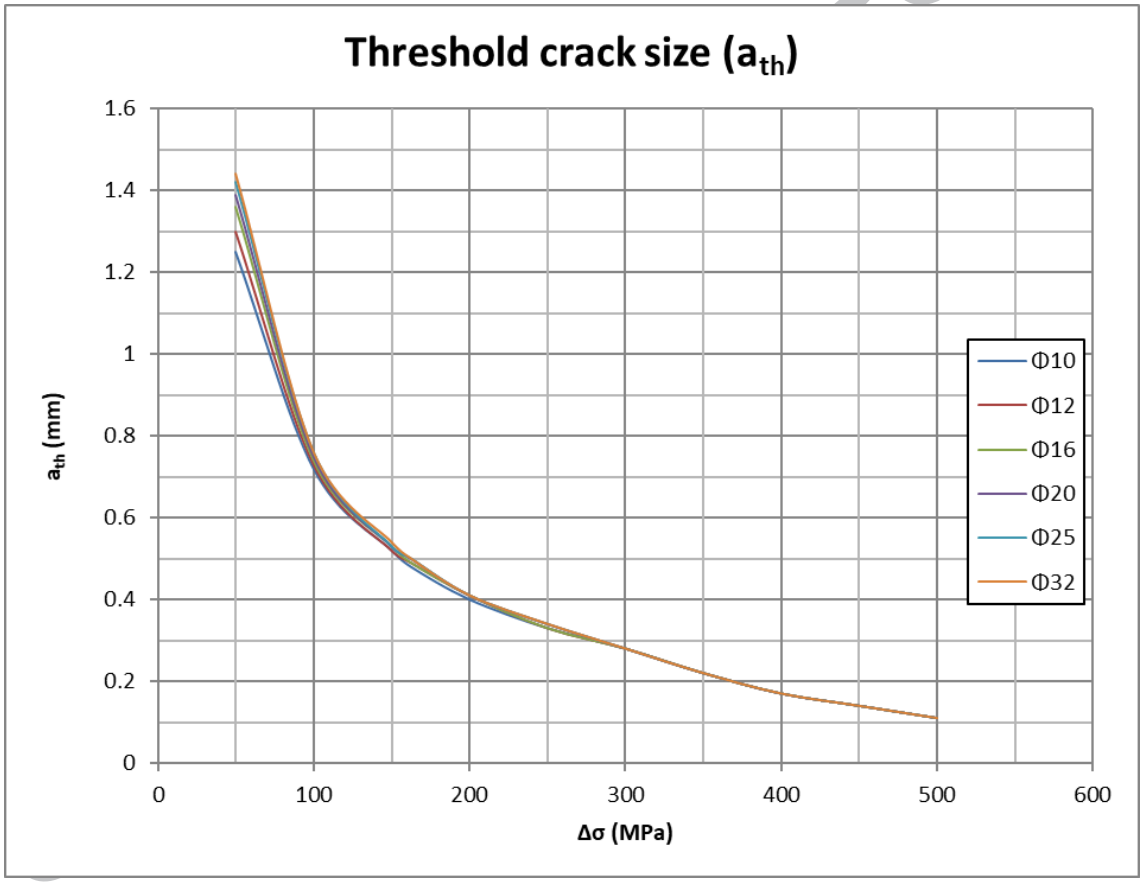

Figure 2: Minimum threshold crack size.

Similarly, once a critical crack size has been reached, the crack will suddenly propagate out of control and fatigue failure will occur. The critical crack size (a_{cr}) is defined in eq. (16), which was defined on the same basis as (a_{th}). The values obtained, for different diameters, are summarized in Table 4 and plotted in Figure 3 [40]. This time, $Y_{cr}=Y(a_{cr})$ as defined in (9) and (σ_{sup}) is the higher tensile stress of the cycle, while K_{IC} was previously defined in Table 1, according to [34].

$$a_{cr} = \frac{1}{\pi}\left(\frac{\Delta K_{IC}}{Y_{cr}\sigma_{sup}}\right)^2 24 \qquad (16)$$

Table 4: Critical crack size values, a_{cr} [mm].

a_{cr}						
Δσ	**Φ10**	**Φ12**	**Φ16**	**Φ20**	**Φ25**	**Φ32**
50	6.3	7.34	9.31	11.16	13.33	16.15
100	6.11	7.11	8.98	10.74	12.78	15.43
150	5.93	6.88	8.67	10.34	12.27	14.75
162.5	5.88	6.83	8.6	10.24	12.14	14.59
200	5.76	6.67	8.38	9.96	11.78	14.12
250	5.6	6.47	8.11	9.61	11.33	13.52
300	5.44	6.29	7.85	9.27	10.9	12.96
350	5.3	6.11	7.6	8.95	10.5	12.43
400	5.16	5.93	7.36	8.65	10.11	11.93
450	5.02	5.77	7.13	8.36	9.75	11.46
500	4.89	5.61	6.92	8.09	9.4	11.01

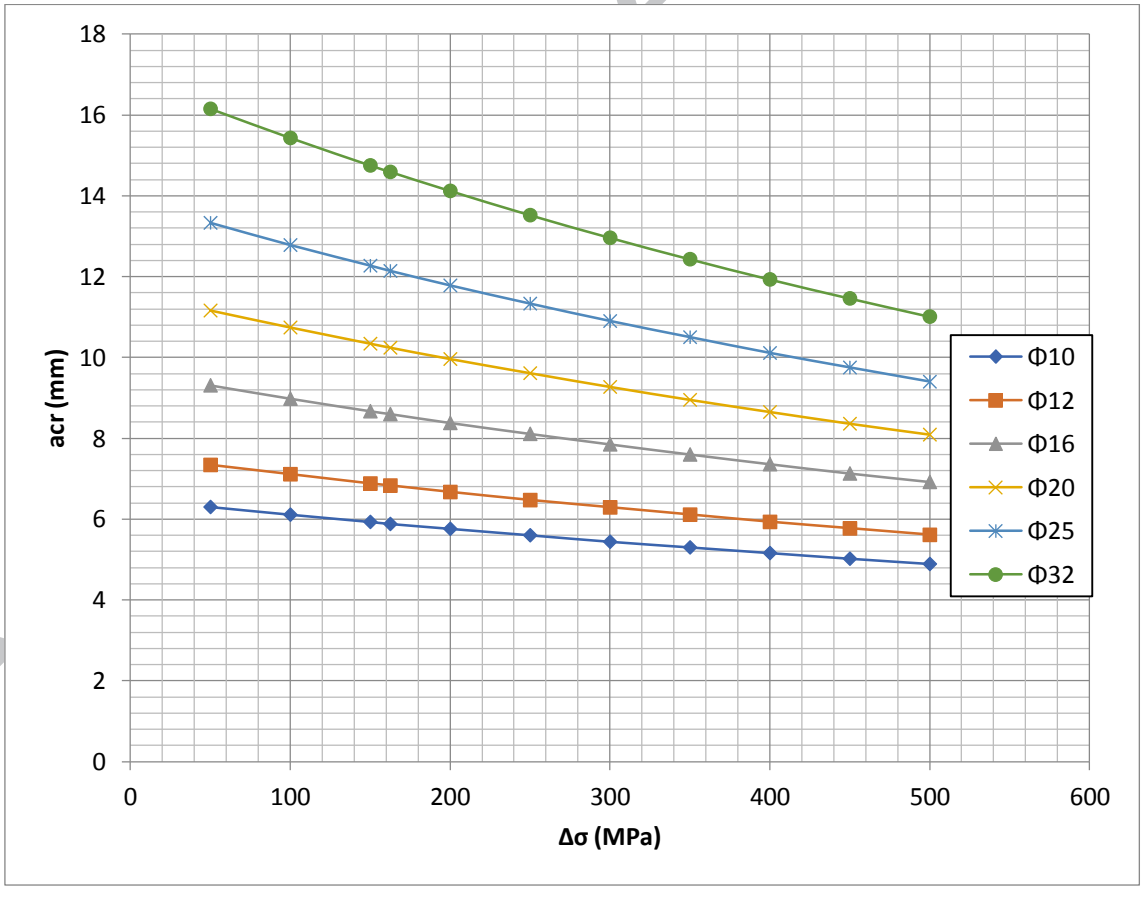

Figure 3: Critical crack size, a_{cr} [mm].

3.3 Deriving S-N Curves for an inert environment

Now, with the data summarized in Table 1 to Table 4, it is possible to derive the number of cycles until fracture for each diameter (Φ) considering different tensile ranges (Δσ). Thus, Figure 4 shows the number of cycles until failure at different stress ranges and rebar diameters. The performance of all the bars is similar, showing parallel lines from different initial ordinates. Besides, the larger the diameter, the higher the resistance to fatigue failure. This fact is close to the prediction of Eurocode 2 EN 1992-1-1:2013 [22]. The differences in fatigue resistance come from the different values of the geometry factor, Y(a), when changing the diameter (Φ), leading to different crack sizes (a_{cr}) that limit the number of cycles from relatively similar initial crack sizes (a_{th}).

Just for note, it is worth mentioning that S-N curves derived in this way are semi-empirical. The base S-N curves for inert environment in standards are derived from mechanical fatigue testing. Besides, the material constants A and m are obtained by testing, the geometrical factor Y(a) is obtained by testing or, in some cases, by FEM simulation after mechanical characterization of material. The mean frequency f is obtained in real cases as the root square of the quotient of 4th order momentum divided by the 2nd order momentum of power spectral density function PSD obtained by direct measurement. Finally, the mean corrosion rate is measured with a corrosimeter. Therefore, the process is semi-empirical in the sense that it is based on direct measurement of some physical properties, but the modified S-N curve is derived theoretically by this methodology thereafter.

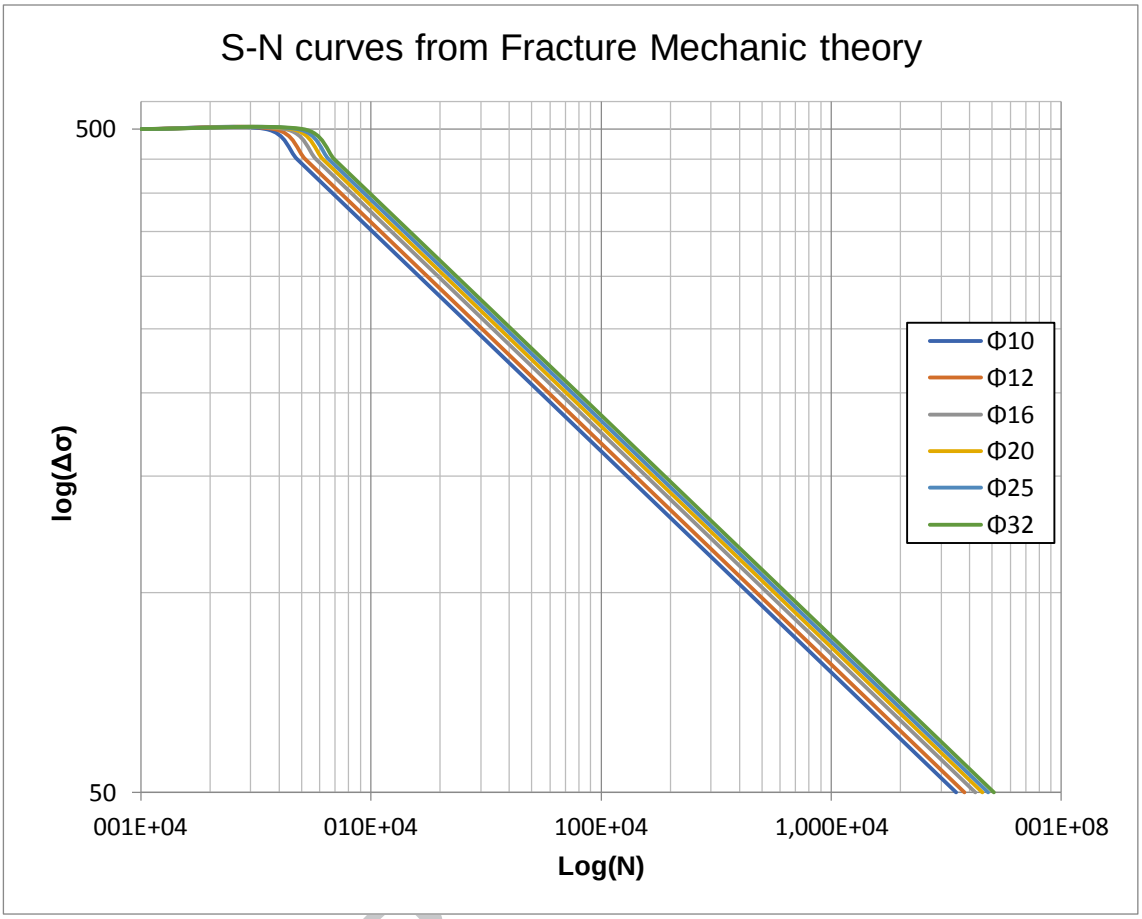

Figure 4: S-N curves derived from fracture mechanics theory in double logarithm scale.

Table 5: Slope (m) and fatigue limit ($\Delta\sigma_L$) depending on rebar diameter (Φ)

Φ[mm]	10	12	16	20	25	32
m [-]	-1/3	-1/3	-1/3	-1/3	-1/3	-1/3
$\Delta\sigma_L$ [MPa]	163.45	167.95	174.08	178.11	181.64	185.02

As a comparative study and to gather further information, S-N curves are drawn in Figure 5 for ϕ25 considering Fracture Mechanics for an inert environment and EN 1992-1-1:2013 [22] for inert and corrosive environments. The greater difference between the Fracture Mechanics line and the one obtained from EN 1992-1-1:2013 [22], is the slope of the line. As summarized in Table 5, the Fracture Mechanics theory defines a slope of -1/3 and the regulations define a slope of -1/5, this means that Fracture Mechanics define a more critical law than regulation. It must be pointed out that the curves are plotted for 225 MPa mean tensile stress and ultimate limit states define a maximum tensile stress of around 60-65% of yield stress. Considering all the aspects, the common working tensile stress amplitude is 162.5MPa or lower. Observing Figure 5 and in view of that tensile ratio, if we also consider a common tensile stress amplitude, then the line representing EN 1992-1-1:2013 [22] is not on the side of safety.

Figure 5 also shows the S-N curve considering a corrosive marine atmosphere (XS1). Paying attention to the difference obtained for an inert environment, the following step is to define the S-N curves for an XS1 environment by applying the Fracture Mechanics law.

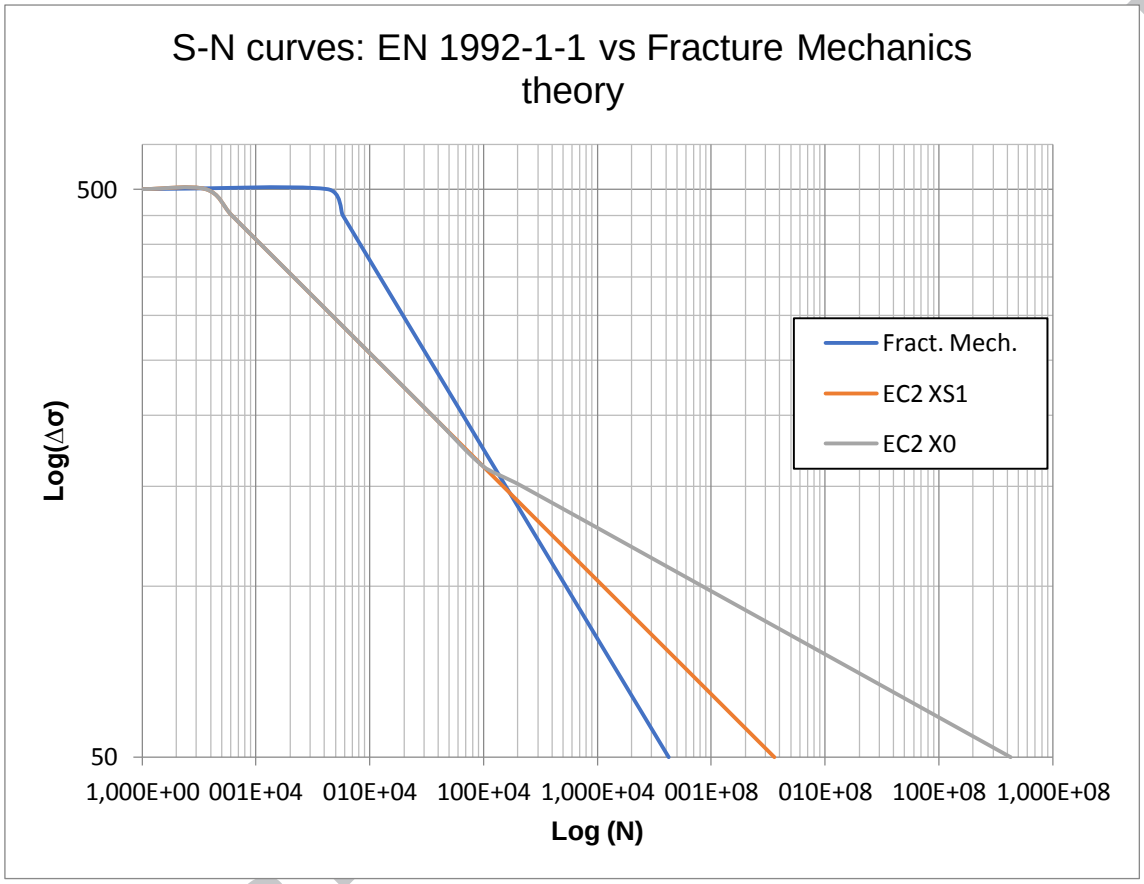

Figure 5: A comparative analysis of SN curves obtained from: Fracture Mechanics in an inert environment and UNE-EN 1992-1-1 in an inert environment and in an XS1 marine atmospheric corrosion mode.

Finally, despite the limitation disclosed in the Eurocode 2 [22] regarding the S-N curve slope and the fatigue limit, the seminal ECCS Document [23] on fatigue, specifies a slope of 1/3 and a fatigue limit of 100 MPa at $2 \cdot 10^6$ cycles. Figures that are more consistent with theory, as 1/5 is more suitable for rods/bolts and the like under shear stress.

3.3 S-N curves with corrosive environments

Hence, having demonstrated that the S-N curves defined in the standards are less restrictive than those obtained with Fracture Mechanics theory, the following step is to define the S-N curve for fatigue corrosion. Thus, in this study, the XS1 exposure class was considered, which means that the structure would be placed a few kilometres from the coast [32, 22, 41], i.e. marine atmospheric exposure. Under these conditions, the guidelines define a 20μm/year corrosion rate for XS1 exposure conditions. However, in terms of safety, some previous research suggests a factor of 10 for a corrosion rate under marine pitting corrosion [42, 43], which implies a corrosion rate of 200 μm/year. However, the corrosion rate is insufficient to define the corrosion weight in the

corrosion fatigue process, as the service life of the structure and the possible stress ranges must also be considered.

During its service life, a structure will come under different frequencies and stress ranges. A mean frequency value may be obtained, by applying a power spectral density function [44, 45, 46]. However, as real service-life conditions are a priori unknown, the study of the frequencies summarized in Table 6 will be considered for structural engineering applications.

Hence, structures are designed for between 50 and 100 years of service life depending on the usage of the reinforced concrete structure -residential or civil engineering works- and its importance. As previously mentioned, the corrosion factor depends on frequency, so the corrosion rate is higher at lower frequencies. Thus, some structural details are defined for millions of cycles during their service life and others for hundreds of millions of cycles. Four possible frequencies are defined in Table 6.

Table 6: Frequencies [Hz] under consideration, depending on the length and the minimum number of cycles throughout the service life.

Frequency		Cycles	
		10^6	10^8
Service life	100	f_1	f_3

Figure 6 summarizes the cycles up until failure for each combination of diameter (Φ), stress range (Δσ) and frequency (f), from f_1 to f_4 in a) to d) respectively. The graphs are plotted in double logarithm scale for comparison with data from an inert environment. Comparing Figure 4 and Figure 6, it becomes evident that corrosion modifies the fatigue process when comparing results with the straight lines defined in Figure 4.

Figure 5, the S-N curves are now non-linear and the number of cycles until failure drastically decreases when the coupled corrosion fatigue is analysed. The drop is higher for lower tensile stress ranges. For example, the fatigue resistance of a 25 mm diameter rebar and a stress range of 162.5 MPa will decrease from 1,400,000 cycles to 220,000, implying a fatigue resistance reduction of 84%.

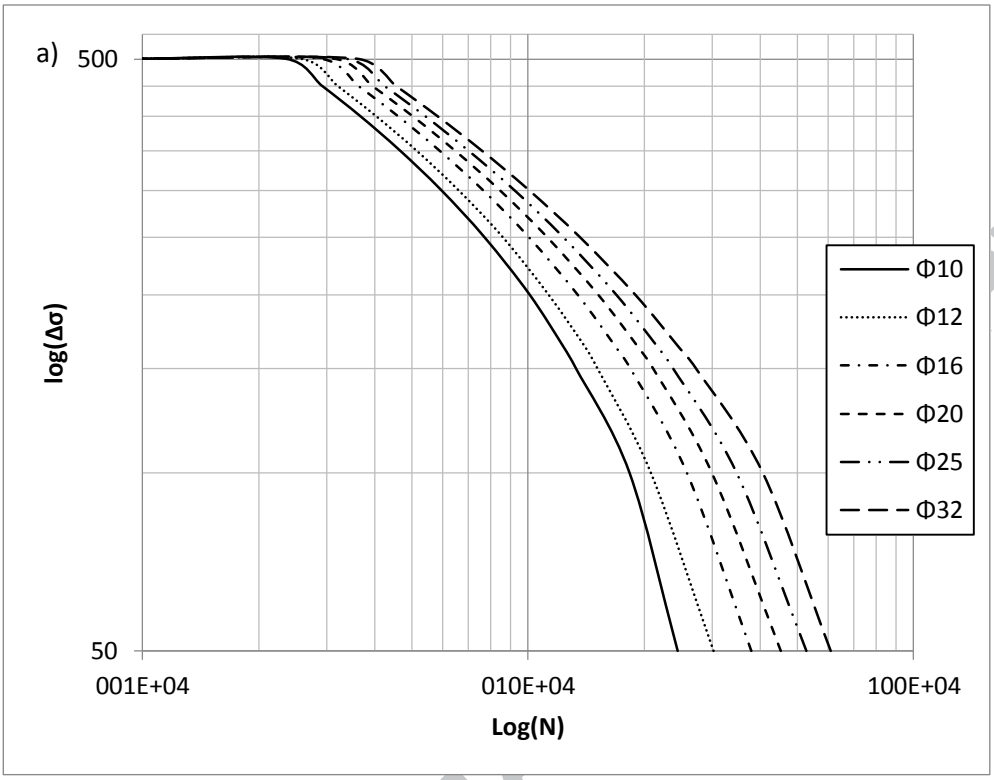

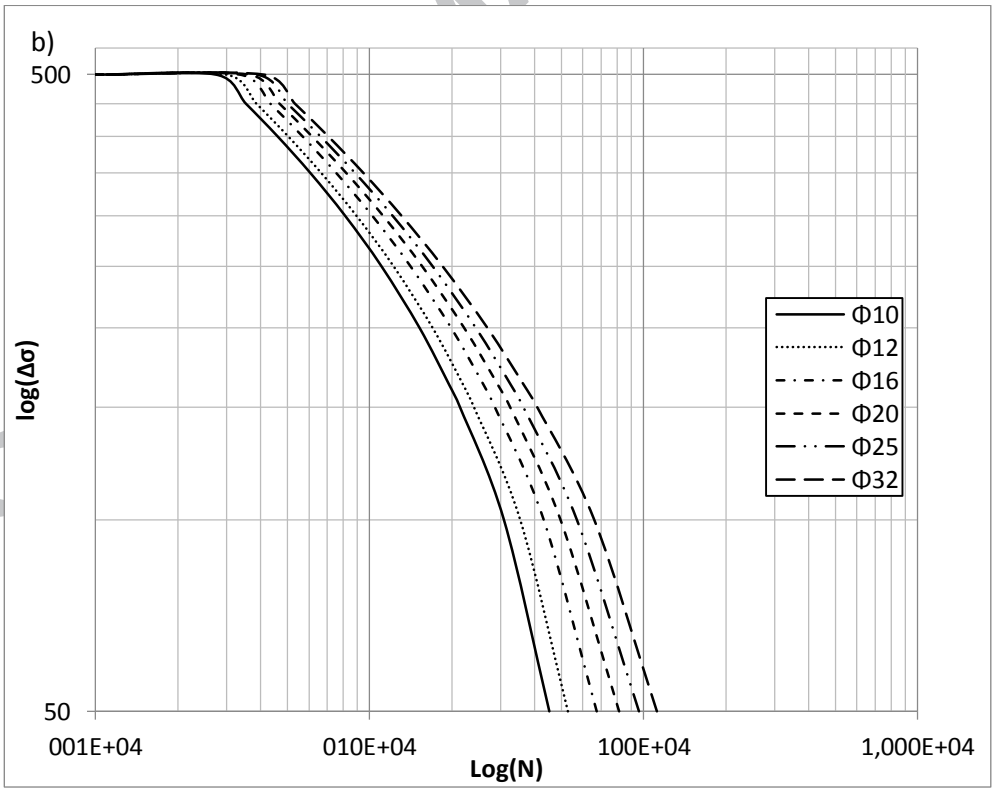

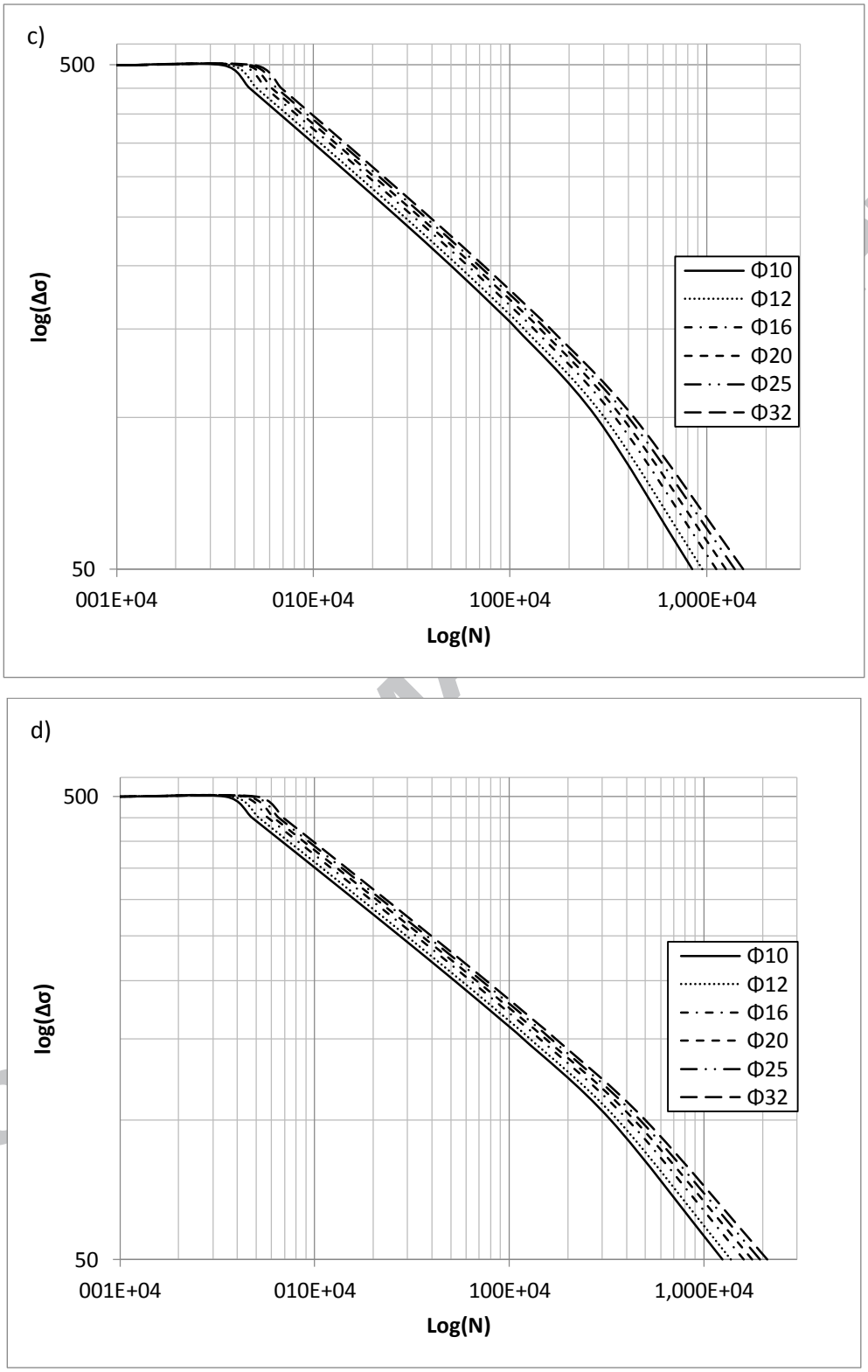

Figure 6: S-N curves for a corrosive marine atmosphere (XS1 exposure class) with a corrosion rate of 0.2 mm/year, and at different frequencies: a) f_1, b) f_2, c) f_3, and d) f_4.

4. Corrosion Pushing Factor

In this study, a corrosion pushing factor is defined for application in conjunction with the Palmgren-Miner linear rule [8, 9], for the definition of coupled fatigue-corrosion damage, in the same way as presented in the case of the loading sequence effect [10]. This development will be useful to extend standard applications of the plain rule, which is widely used for structural engineering purposes, on corrosive environment scenarios.

4.1 Consideration of the variables

Both the fatigue behaviour and the corrosion pushing factor alike depend on the diameter (Φ), the exposure class (XS1, in this case) and the load frequency (f). Thus, the data are separately presented in Figure 7, showing results for the two diameters ϕ 10 and ϕ 32 in the two environments, and in Figure 8, varying the frequencies for ϕ 10 (Figure 8 a) and ϕ 32 (Figure 8 b).

Thus, diameter size (Φ) behaved in the same way in each environment, showing how larger diameters work better than lower ones. Nevertheless, fatigue resistance decreased from 90% to 30% as the stress range increased. Finally, Figure 8 demonstrates the fact that corrosion influence is higher at lower frequencies, as the resulting curves are further displaced from the reference curve in an inert environment.

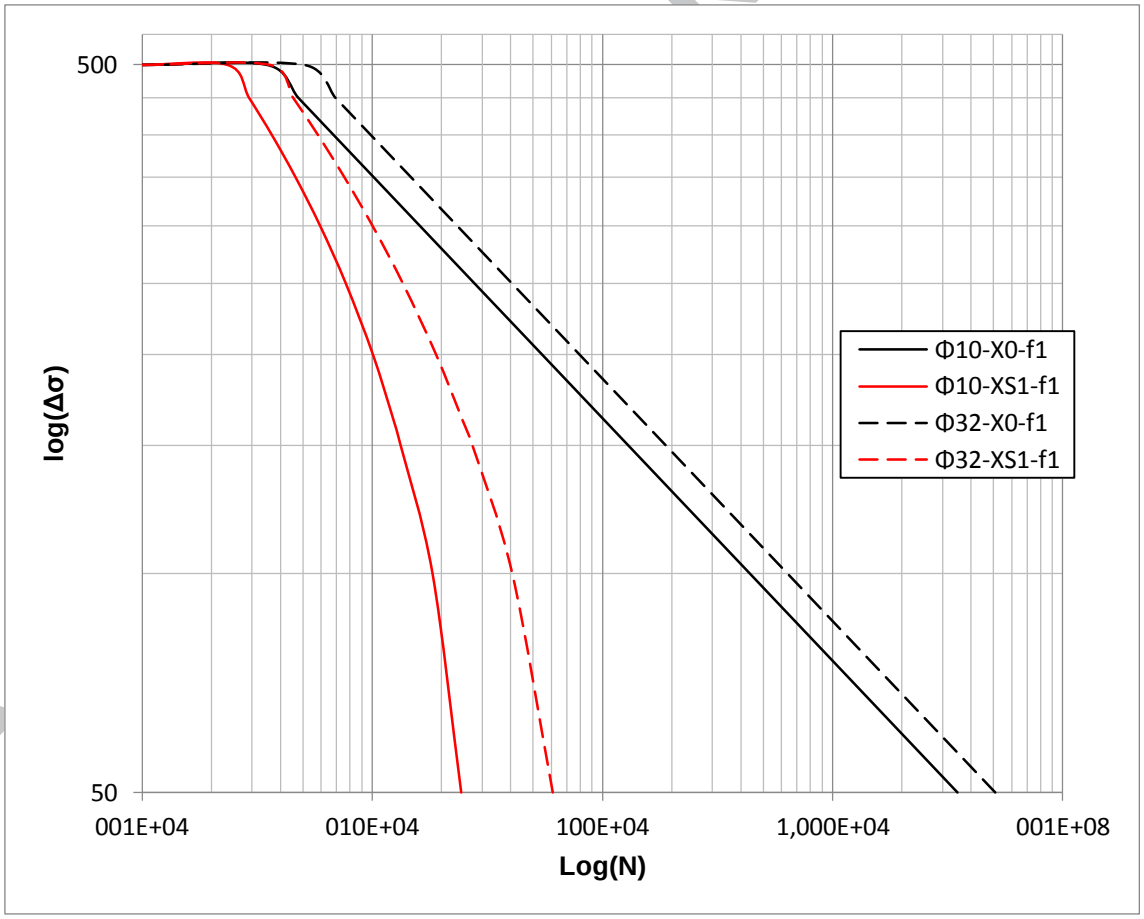

Figure 7 Corrosion fatigue behaviour: comparative study of ϕ 10 and ϕ 32 in an inert (I) environment and an XS1 exposure class.

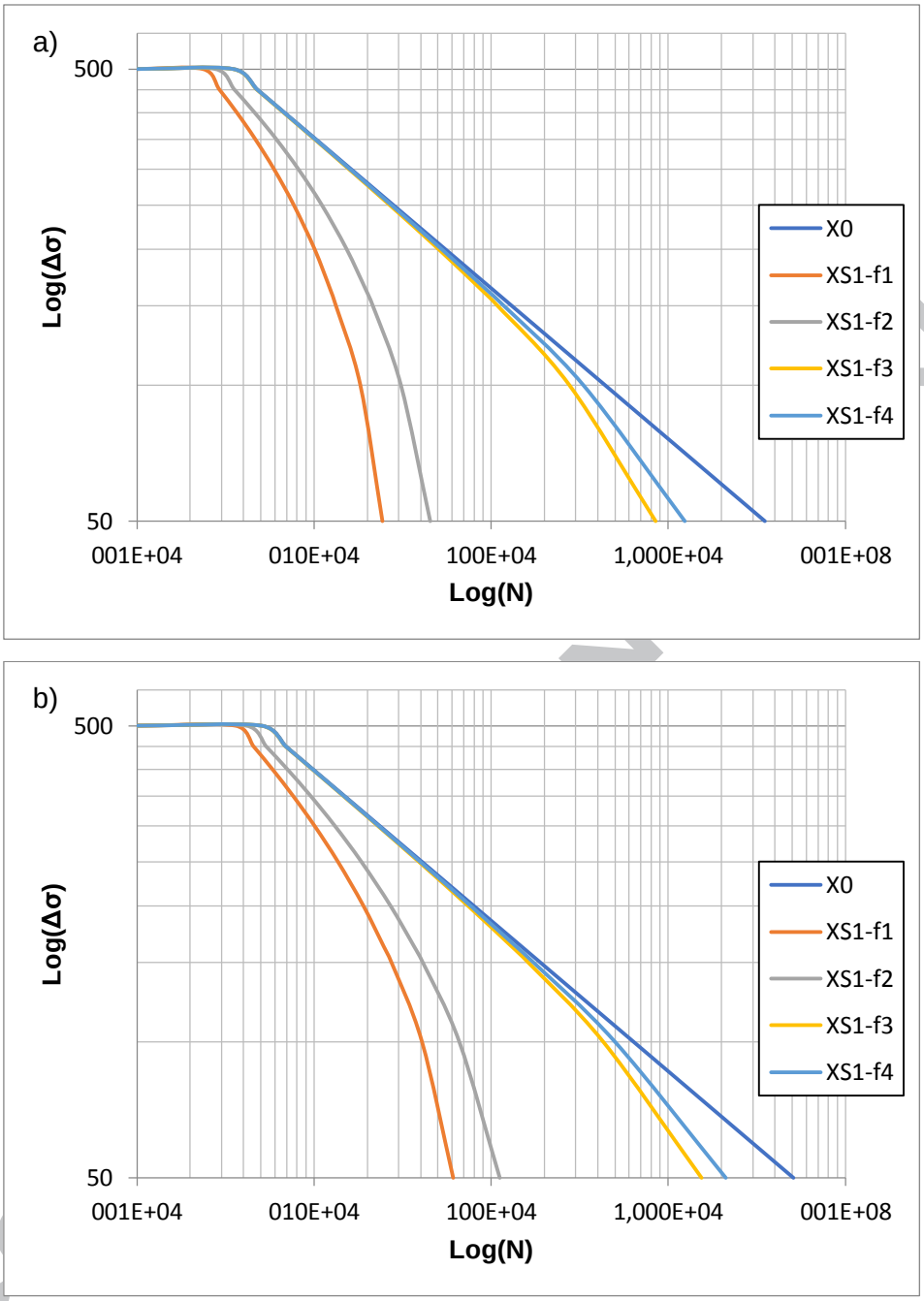

Figure 8: Influence of exposure class (X0, XS1) and frequencies on: a) ϕ 10 diameter rebars; and, b) ϕ 32 diameter rebars

4.2 Deriving the Mean Corrosion Pushing Factor

The pushing factor defined in eq. (12) depends on several variables such as the crack size, geometry factor, frequency, etc. Hence, the essential use of fracture mechanics to derive the damage accumulation level. Even if eq. (12) is an accurate method of defining the pushing factor, it is not in keeping with the engineering rule of keeping it plain and simple to be useful, which, even if not so accurate, guides the fatigue calculations in the Palmgren-Miner rule, among others [8, 9]. This handicap encourages the definition of a simpler mean corrosion-pushing factor (F_{MCP}). The

defined (F_{MCP}) must be capable of representing any crack size (from a_0 to a_{cr}) and any service life condition (frequencies, corrosion rate, stress amplitude…), offering conservative values, and independent of any variable defined by fracture mechanics theory. Besides, since it is derived from the quotient of required cycles causing the crack to grow from a_{th} to a_{cr} under inert environment to the amount needed to cause the same crack growth under corrosive environment, calculated by an iterative method with steps of mechanical and corrosive crack propagation, this methodology is compatible with a Palmgren-miner summation with lower and safer limits, such as 0,7 or others according regulations [47].

Thus, a (F_{MCP}) for steel rebars is proposed in this section. Table 7 to Table 12 summarize (F_{MCP}) the proposed values for different reinforcement diameters (Φ) under different stress ranges (Δσ) and frequencies (f). Each (F_{MCP}) is obtained by dividing the number of cycles until failure in an inert environment by the number of cycles until failure in an XS1 exposure class for each stress range (Δσ) and frequency (f). This factor can be used to define the corrosion fatigue damage at each stage: multiplying (F_{MCP}) by the quotient of number of cycles (N_i) to final number of cycles ($N_{f,i}$).

The total cumulative corrosion fatigue damage will be obtained as defined in eq. (21):

$$D_{CF} = \sum_{1}^{N} F_{MCP} \cdot \frac{N_i}{N_{f,i}} \tag{21}$$

Table 7 Mean Corrosion-Pushing Factor values defined for ϕ 10 reinforcements.

Φ10	**Δσ**										
f	**50**	**100**	**150**	**162.5**	**200**	**250**	**300**	**350**	**400**	**450**	**500**
f_1	143.29	23.88	9.74	8.22	5.42	3.63	2.72	2.19	1.86	1.64	1.48
f_2	77.15	14.13	6.04	5.20	3.58	2.52	1.98	1.67	1.47	1.35	1.26
f_3	4.13	1.58	1.20	1.16	1.09	1.05	1.03	1.02	1.01	1.01	1.01
f_4	2.82	1.32	1.10	1.08	1.04	1.02	1.01	1.01	1.01	1.00	1.00

Table 8 Mean Corrosion-Pushing Factor values defined for ϕ 12 reinforcements.

Φ12	**Δσ**										
f	**50**	**100**	**150**	**162.5**	**200**	**250**	**300**	**350**	**400**	**450**	**500**
f_1	125.37	22.77	9.28	7.83	5.25	3.53	2.66	2.15	1.83	1.62	1.47
f_2	71.64	13.36	5.83	5.01	3.48	2.47	1.95	1.65	1.46	1.34	1.26
f_3	4.00	1.57	1.19	1.16	1.09	1.04	1.03	1.02	1.01	1.01	1.01
f_4	2.76	1.31	1.10	1.08	1.04	1.02	1.01	1.01	1.01	1.00	1.00

Table 9 Mean Corrosion-Pushing Factor values defined for ϕ16 reinforcements.

Φ16	**Δσ**										
f	**50**	**100**	**150**	**162.5**	**200**	**250**	**300**	**350**	**400**	**450**	**500**
f_1	111.33	20.45	8.49	7.26	4.91	3.36	2.56	2.09	1.79	1.59	1.45
f_2	62.62	12.22	5.45	4.70	3.32	2.39	1.90	1.62	1.44	1.33	1.25
f_3	3.78	1.54	1.19	1.15	1.08	1.04	1.03	1.02	1.01	1.01	1.01
f_4	2.64	1.30	1.10	1.08	1.04	1.02	1.01	1.01	1.01	1.00	1.00

Table 10 Mean Corrosion-Pushing Factor values defined for ϕ20 reinforcements.

Φ20	**Δσ**										
f	**50**	**100**	**150**	**162.5**	**200**	**250**	**300**	**350**	**400**	**450**	**500**
f_1	100.20	18.91	7.94	6.81	4.66	3.23	2.48	2.04	1.76	1.57	1.44
f_2	55.67	11.39	5.13	4.47	3.19	2.32	1.86	1.60	1.43	1.32	1.24
f_3	3.62	1.52	1.18	1.14	1.08	1.04	1.02	1.02	1.01	1.01	1.01
f_4	2.56	1.29	1.09	1.08	1.04	1.02	1.01	1.01	1.01	1.00	1.00

Table 11 Mean Corrosion-Pushing Factor values defined for ϕ25 reinforcements.

Φ25	**Δσ**										
f	**50**	**100**	**150**	**162.5**	**200**	**250**	**300**	**350**	**400**	**450**	**500**
f_1	91.09	17.26	7.47	6.42	4.43	3.11	2.41	1.99	1.73	1.55	1.42
f_2	50.10	10.54	4.88	4.26	3.07	2.26	1.83	1.57	1.41	1.31	1.23
f_3	3.47	1.50	1.17	1.14	1.08	1.04	1.02	1.02	1.01	1.01	1.01
f_4	2.48	1.28	1.09	1.07	1.04	1.02	1.01	1.01	1.01	1.00	1.00

Table 12 Mean Corrosion-Pushing Factor values defined for ϕ32 reinforcements.

Φ32	**Δσ**										
f	**50**	**100**	**150**	**162.5**	**200**	**250**	**300**	**350**	**400**	**450**	**500**
f_1	83.42	15.64	6.90	5.99	4.19	2.98	2.33	1.95	1.70	1.53	1.41
f_2	45.50	9.62	4.59	4.04	2.94	2.20	1.79	1.55	1.40	1.29	1.22
f_3	3.30	1.48	1.17	1.14	1.08	1.04	1.02	1.02	1.01	1.01	1.01
f_4	2.40	1.27	1.09	1.07	1.04	1.02	1.01	1.01	1.01	1.00	1.00

5. Case study

A steel rod is proposed as a case study, to demonstrate the feasibility of this method. The principal advantage is that its geometry is very similar to such elements as rebars, bolts, cables and rod-shaped suspension cables. A reinforced concrete bridge is assumed for the purposes of the study at a few kilometres from the coast (XS1). Table 13 defines the boundary conditions for the case study.

Table 13 Boundary conditions for the analysis

Diameter [mm]	25
Yield stress [MPa]	500
Maximum tensile stress [MPa]	300
Minimum tensile stress [MPa]	150
Tensile amplitude [MPa]	150
Mean tensile [MPa]	225
Service life [years]	100
Load frequency [Hz]	$3.17 \cdot 10^{-4}$
Corrosion rate [μm/year]	200

Reinforcing steel must meet the criteria defined in EN 10080 [33] according to EN-1992 [22] specifications. Both standards specify that the fatigue life of reinforcing steel in an inert environment, is $2 \cdot 10^6$ cycles. In contrast, considering an exposure class of XS1, the boundary conditions defined in Table 13 match the conditions shown in Table 11, which summarize the corrosion pushing factor for a rebar diameter of ϕ 25. In the study, a frequency of $3.17 \cdot 10^{-4}$ Hz (f_1) and a 150 MPa tensile range is defined, which as shown in Table 11 yields a corrosion pushing factor of 7.47, and a corrosion fatigue life of 267,737 cycles. This result implies a reduction in fatigue resistance of 86.61%.

6. Conclusions

1. Fatigue caused by mechanical processes is related to the number of loading cycles while corrosion mechanism is related to the exposure time of structural elements.
2. Load cycles and exposure times are linked through load-cycle frequencies. The higher the load-frequency, the lower the corrosion effect.
3. The Corrosion Pushing Factor is defined as the ratio of the number of load cycles causing crack propagation in a purely mechanical process, to the number of mechanical cycles in a coupled corrosion-fatigue condition to predict the same crack size. It can therefore, be said that in a corrosion fatigue process, corrosion adds virtual load cycles, ΔN_C.
4. The method that has been presented permits the determination of the fatigue service life in a corrosion-coupled fatigue process. The crack propagation rate is higher when the synergic action of both fatigue and corrosion is considered than when the sum of each independent action is assessed.
5. Based on the Palmgren-Miner linear rule, the Mean Corrosion Pushing Factor F_{MCP} enables the determination of corrosion fatigue damage from mechanical fatigue S-N curves.
6. The theory that has been developed in this paper is consistent with the behaviour of fatigue processes observed in the presence of a corrosive environment and a set of given load frequencies.

7. References

[1] Det Norske Veritas As, *Offshore Standard DNV-OS-J101 Design of Offshore Wind Turbine Structures,* DNV GL AS, 2014.

[2] Det Norske Veritas As, *DNV-RP-C203 Fatigue Design of Offshore Steel Structures,* DNV GL AS, 2011.

[3] British Standards Institution, *BS EN ISO 19902 Petroleum and natural gas industries. Fixed steel offshore structures,* BSI, 2013.

[4] C. Sonsino, «Comparison of different local design concepts for the structural durability assessment of welded offshore K-nodes,» *International Journal of Fatigue,* vol. 34, nº 1, pp. 27-34, 2012.

[5] European Standard, *Eurocode 3: Design of steel structures - Part 1-9: Fatigue,* European Standard, 2005.

[6] AISC American Institute of Steel Construction, *Fatigue and Fracture Control in Steel Structures,* AISC, 2007.

[7] A. Wöhler, «Über die festigkeitsversuche mit eisen und stahl,» *Zeitschrift für,* vol. 20, pp. 73-106, 1870.

[8] A. Palmgren, «Die lebensdauer von kugellagern,» *Verfahrrenstechinik,* vol. 58, pp. 39-341, 1924.

[9] M. Miner, «Cumulative damage in fatigue,» *Journal of Applied Mechanics,* vol. 67, pp. A159-A164, 1945.

[10] I. Calderon-Uriszar-Aldaca y M. V. Biezma, «A plain linear rule for fatigue analysis under natural loading considering the squence effect,» *International Journal of Fatigue,* vol. 103, pp. 386-394, 2017.

[11] C. Wang, J. Xiong, R. Shenoi, M. Liu y J. Liu, «A modified model to depict corrosion fatigue crack growth behavior for evaluating residual lives of aluminum alloys,» *International Journal of Fatigue,* vol. 83, pp. 280-287, 2016.

[12] J. Toribio, J. C. Mateos y B. Gonzalez, «Corrosion-Fatigue Crack Growth in Plates: A Model Based on the Paris Law,» *Materials,* vol. 10, pp. 439-448, 2017.

[13] A. Cheng y N.-Z. Chen, «Corrosion fatigue crack growth modelling for subsea pipeline steels,» *Ocean Engineering,* vol. 142, pp. 10-19, 2017.

[14] B. Sun, «A continuum model for damage evolution simulation of the high strength bridge wires due to corrosion fatigue,» *Journal of Constructional Steel Research,* vol. 146, pp. 76-83, 2018.

[15] F. Gallerneau, Etude et modélisation de l'endommagement d'un superalliage monocristalin revêtu pour aube de turbine, 1995, University of Paris.

[16] C. Kortovich, «Corrosion Fatigue of 4340 and D6AC steels below KISCC,» de *Proceedings of the 1974 Triservice Conference on Corrosion of Military Equipment*, Wright-Patterson Air Force Base, 1975.

[17] D. Dawson y R. Pelloux, «Corrosion fatigue crack growth of titanium alloys in aqueous environments,» *Metallurgical and Materials Transactions A,* vol. 5A, pp. 723-731, 1974.

[18] P. Pao, W. Wei y R. Wei, «Effects of frequency on fatigue crack growth response of AISI 4340 steel in water vapor,» de *Proceedings, Symposium on Environment-Sensitive Fracture of Engineering Materiales*, Chicago, IL, 1979.

[19] R. Wei y G. Shim, «Fracture mechanics and Corrosion Fatigue,» de *Corrosion Fatigue: Mechanics, metallurgy, electrochemistry and engineering*, Baltimore, MD: ASTM, 1984, pp. 5-25.

[20] P. Paris y F. Erdogan, «A Critical Analysis of Crack Propagation Laws,» *Journal of Basic Engineering,* vol. 85, pp. 528-534, 1963.

[21] A. Griffith, «The phenomena of rupture and flow in solids,» *Philosophical Transactions of the Royal Society of London,* vol. 221, pp. 163-198, 1921.

[22] CEN Comité Européen de Normalisation, EN 1992-1-1:2013, Eurocode 2: Design of concrete structures - Part 1.1: General rules and rules for buildings, Brussels, Belgium: CEN Comité Européen de Normalisation, 2013.

[23] European Convention for Constructional Steelwork. Technical Committee 6, Fatigue, Recommendations for the fatigue design of steel structures / ECCS - Technical Committee 6 - Fatigue., vol. 43, G. Secretariat, Ed., Brussels: ECCS, 1985.

[24] European Convention for Constructional Steelwork, «CCS. Seismic design. Recommended testing procedure for assessing the behaviour of structural steel elements under cyclic loads.,» 1986.

[25] I. Fernandez, J. M. Bairán y A. R. Marí, «Corrosion effects on the mechanical properties of reinforcing steel bars. Fatigue and r–e behavior,» *Construction and Building Materials,* vol. 101, pp. 772-783, 2015.

[26] J. R. Donahue y J. T. Burns, «Effect of chloride concentration on the corrosion–fatigue crack behavior of an age-hardenable martensitic stainless steel,» *International Journal of Fatigue,* vol. 91, pp. 79-99, 2016.

[27] *BS 7910:2013 Guide to methods for assessing the acceptability of flaws in metallic structures,* London: BSI, 2013.

[28] M. Hirt, R. Bez y A. Nussbaumer, Construction métallique: notions fondamentales et méthodes de dimensionnement,nouvelle édition revue et adaptée aux nouvelles normes de structures, vol. 10, Lausanne, Switzerland: EPFL, 2006.

[29] L. Deng, W. Yan y L. Nie, «A simple corrosion fatigue design method for bridges considering the coupled corrosion-overloading effect,» *Engineering Structures,* vol. 178, pp. 309-317, 2019.

[30] D. H. Yang, T.-H. Yi y H.-N. Li, «Coupled Fatigue-Corrosion Failure Analysis and Performance Assessment of RC Bridge Deck Slabs,» *Journal of Bridge Engineering,* vol. 22, nº 10, 2017.

[31] ASM International, *ASM Handbook volume 19 fatigue and fracture,* 1997.

[32] Ministerio de Fomento, EHE-08 Instrucción de hormigón estructural con comentarios de los miembros de la comisión permanente del hormigón, Madrid, Spain: Centro de Publicaciones de la Secretaría General Técnica, 2010.

[33] CEN Comité Européen de Normalisation, *UNE-EN 10080:2006 Steel for the reinforcement of concrete - Weldable reinforcing steel - General,* Madrid: CEN Comité Européen de Normalisation, 2006.

[34] A. Herwig, Reinforced concrete bridges under increased railway loads – fatigue behavior and safety measures, Lausanne, Switzerland: Ph.D. Dissertation, EPFL, 2008.

[35] R. Stephens, A. Fatemi, R. Stephens y H. Fuchs, Metal fatigue in engineering, New York, NY: Wiley Interscience, 2001.

[36] N. Dowling, Mechanical behavior of materials, New Jersey, NJ: Prentice Hall, 1993.

[37] J. Newman, «Fatigue and Crack-growth Analyses under Giga-cycle Loading on Aluminum Alloys,» *Procedia Engineering,* vol. 101, pp. 339-346, 2015.

[38] J. Schivje, «Fatigue of structures and materials in the 20th century and the State of the Art.,» *International Journal of Fatigue,* vol. 25, pp. 679-702, 2003.

[39] I. Calderón , M. V. Biezma, A. Matanza y M. Calderón, «Modelo discreto de acumulación de daño de fatiga mecánica y fatiga por corrosión acopladas en medio ambiente agresivo,» de *Anales de Mecánica de la Fractura*, Bilbao, Spain, 2012.

[40] I. Calderon-Uriszar-Aldaca, «Fatigue of Structural Elements by Random Dynamic Actions in Aggresive Environment,» *University of Cantabria,* 2014.

[41] CEN Comité Européen de Normalisation, UNE-EN 206:2013+A1:2018 , Concrete - Specification, performance, production and conformity, Madrid, Spain: CEN

Comité Européen de Normalisation, 2018.

[42] K. Tuutti, «Corrosion of steel in concrete,» de *Cement och betonginstitutet*, Stockholm, Sweden, 1982.

[43] J. González, C. Andrade, C. Alonso y S. Feliú, «Comparison of rates of general corrosion and maximum pitting penetration on concrete embedded steel reinforcements,» *Cement and Concrete Research,* vol. 25, nº 2, pp. 257-264, 1995.

[44] J. Bendat y A. Piersol, «Engineering Applications of Correlation and Spectral Analysis,» *Wiley-Interscience,* pp. 47-64, 1980.

[45] R. Clough y J. Penzien, Dynamics of structures, 3 ed., Berkeley, CA: Computers & Structures, Inc., 2003.

[46] D. Thorby, Structural dynamics and vibration in practice, 1 ed., Oxford, UK: Elsevier,, 2008.

[47] ASTM STP 1439, Principles of Variable Amplitude Fatigue Design and Testing, ASTM International, 2005, pp. 3-23.